Transient behavior of the Asian summer monsoon anticyclone associated with eastward eddy shedding

Xinyue Wang[1], William J. Randel[2], Laura L Pan[3], Yutian Wu[4], and Pengfei Zhang[5]

[1]National Center for Atmospheric Research
[2]National Center for Atmospheric Research (UCAR)
[3]National Center for Atmospheric Research (NCAR)
[4]Lamont-Doherty Earth Observatory of Columbia University
[5]University of California Los Angeles

November 22, 2022

Abstract

The Asian monsoon anticyclone (AMA) exhibits a trimodal distribution of sub-vortices and the western Pacific is one of the preferred locations. Amplification of the western Pacific anticyclone (WPA) is often linked with eastward eddy shedding from the AMA, although the processes are not well understood. This study investigates the dynamics driving eastward eddy shedding associated with the emergence of the WPA in the upper troposphere and lower stratosphere on synoptic scales. Using reanalysis data during 1979 to 2019, our composite analysis reveals that amplified WPA events are closely related to the upstream Silk Road (SR) wave-train pattern over mid-latitude Eurasia as identified in previous studies. The quasi-stationary eastward propagating eddies result from baroclinic excitation along the westerly jet, as identified by coherent eddy heat fluxes and relaxation of the low-level temperature gradient. The upper-level westerly jet is important in determining the longitudinal phase-locking of wave trains, which are anchored and amplify near the jet exit. Occasionally enhanced convection near the Philippines also triggers anticyclonic eddies that propagate upward and northeastward via the Pacific-Japan (PJ) pattern, forming the WPA in the upper troposphere. Correlation analysis suggests that the SR and PJ mechanisms are not physically correlated.

Transient behavior of the Asian monsoon anticyclone associated with eastward eddy shedding

Xinyue Wang [1,2], William Randel [2], Laura Pan [2], Yutian Wu [3], Pengfei Zhang [4]

[1]Advanced Study Program, National Center for Atmospheric Research, Boulder, CO, USA
[2]Atmospheric Chemistry Observations and Modeling Lab, National Center for Atmospheric Research, Boulder, CO, USA
[3]Lamont-Doherty Earth Observatory of Columbia University, Palisades, NY, USA
[4]Department of Meteorology and Atmospheric Science, Pennsylvania State University, University Park, PA, USA

Key Points:

- Eastward eddy shedding from the Asian monsoon anticyclone is often associated with the emergence of an isolated western Pacific anticyclone.
- Western Pacific anticyclone is closely related to the Silk Road pattern. Eddies grow along the jet in a baroclinically unstable background.
- Eastward eddy shedding occasionally occurs in association with the Pacific-Japan pattern forced by strong convection near the Philippines.

Abstract

The Asian monsoon anticyclone (AMA) exhibits a trimodal distribution of sub-vortices and the western Pacific is one of the preferred locations. Amplification of the western Pacific anticyclone (WPA) is often linked with eastward eddy shedding from the AMA, although the processes are not well understood. This study investigates the dynamics driving eastward eddy shedding associated with the emergence of the WPA in the upper troposphere and lower stratosphere on synoptic scales. Using reanalysis data during 1979 to 2019, our composite analysis reveals that amplified WPA events are closely related to the upstream Silk Road (SR) wave-train pattern over mid-latitude Eurasia as identified in previous studies. The quasi-stationary eastward propagating eddies result from baroclinic excitation along the westerly jet, as identified by coherent eddy heat fluxes and relaxation of the low-level temperature gradient. The upper-level westerly jet is important in determining the longitudinal phase-locking of wave trains, which are anchored and amplify near the jet exit. Occasionally enhanced convection near the Philippines also triggers anticyclonic eddies that propagate upward and northeastward via the Pacific-Japan (PJ) pattern, forming the WPA in the upper troposphere. Correlation analysis suggests that the SR and PJ mechanisms are not physically correlated.

1 Introduction

The Asian monsoon anticyclone (AMA) is the major circulation pattern in the upper troposphere and lower stratosphere (UTLS) during Northern summer, covering large parts of Eurasia. Relatively high tropospheric trace gases (e.g., water vapor, carbon monoxide, hydrogen cyanide) and aerosol (e.g., sulfate, black carbon) concentrations are confined within the area of anticyclonic circulation, imposing a substantial effect on UTLS composition, and also potentially on the surface weather and climate (Randel et al., 2015; X. Wang et al., 2018; Randel & Park, 2006; Randel et al., 2010; Santee et al., 2017; Höpfner et al., 2019; Vernier et al., 2015; Solomon et al., 2011; Y. Wu et al., 2020).

Understanding the location and movement of the AMA is important for quantifying dynamical and trace gas evolution in the UTLS. Studying the behavior of AMA dates back to Tao and Zhu (1964) who found the opposite movement between the upper-level AMA and mid-level western North Pacific subtropical high in East Asia. Previous studies assuming the anticyclone has a single center reveal that the AMA exhibits a bimodal distribution over Iran and the Tibetan Plateau (Q. Zhang et al., 2002). The details of the bimodal distribution are sensitive to the use of different reanalysis data sets (Nützel et al., 2016), and bimodality is potentially driven by variations in convection (e.g., Garny & Randel, 2013), monsoonal heating (e.g., P. Zhang et al., 2016), orographic effects (Q. Zhang et al., 2002; Liu et al., 2007), and large-scale dynamical variability (Amemiya & Sato, 2020). More recent analyses have highlighted that the AMA is subject to large dynamical variability on synoptic scales, constantly splitting, merging, and shedding anticyclonic eddies westward and eastward (Garny & Randel, 2013, 2016; Pan et al., 2016; P. M. Rupp & Haynes, 2020; Manney et al., 2021). C. J. Hsu and Plumb (2000) showed that an idealized monsoon anticyclone circulation periodically sheds secondary anticyclones due to dynamical instabilities, and observational confirmation of eddy shedding was first shown in Popovic and Plumb (2001). Siu and Bowman (2020) showed that anticyclonic sub-vortices often occur within the AMA at the same time with similar strength. Therefore, consideration of only a single center of the AMA belies the importance of its transient nature and smears out important details.

Recently, Honomichl and Pan (2020) tracked multiple simultaneous maxima of the AMA and identified a third preferred center near 140 E, which is referred to as the western Pacific anticyclone (WPA) or the Bonin high (Enomoto et al., 2003; Enomoto, 2004). Chemical species and low potential vorticity (PV) air within the AMA are shed eastward associated with the emergence of WPA (Vogel et al., 2014; Honomichl & Pan, 2020; Fujiwara et al., 2021). The atmospheric composition and transport pathways associated with the WPA will be systematically investigated in the Asian Summer Monsoon Chemical and Climate Impact Project (ACCLIP) during July-August 2022 (https://www2.acom.ucar.edu/acclip).

While observational studies consistently highlight the chemical signature of the WPA, consensus is yet to be reached on the associated dynamics. This topic has a substantial history. For example, Tao and Zhu (1964) pointed out that the AMA moves in the opposite direction of the western Pacific subtropical high at 500 hPa, modulated by the precipitation in east China. Enomoto et al. (2003) used the primitive-equation model in Hoskins and Rodwell (1995) to study the formation mechanism of the (time-averaged) Bonin high. Their model sensitivity analysis showed that the Bonin high disappears by removing the diabatic cooling over the Asian jet while it still exists at monthly timescale when removing the heating in the western Pacific region. Thus, they emphasized the importance of the external Rossby wave source induced by the cooling due to the monsoon-forced descent over the eastern Mediterranean Sea. The wave disturbances along the Asian jet across Eurasia have since been recognized as the \Silk Road (SR) pattern". In fact, the WPA over Japan was already simulated in Hoskins and Rodwell (1995) but considered to be a model defect after validation against reanalysis data. Further, Enomoto (2004) conducted a composite analysis to study interannual variability of monthly-mean stationary Rossby waves along the subtropical jet (including anticyclonic anomalies over Japan), emphasizing the role of an intensi ed jet in contributing to the eastward group velocity of stationary waves. Yasui and Watanabe (2010) used dry atmospheric general circulation model and identi ed the Silk Road pattern as a part the circumglobal teleconnection. They performed a singular value decomposition (SVD) analysis for the diabatic heating and meridional wind anomalies, and concluded that the heating anomalies over the eastern Mediterranean is most responsible for the formation of the WPA, rather than cooling anomalies induced by the monsoon. P. Rupp and Haynes (2021) used a dry dynamical core model to simulate interactions of the Asian monsoon with baroclinic eddies on the westerly jet. They observed a transition from a steady circulation with westward eddy shedding to an unstable eastward eddy shedding state as the background meridional temperature gradient gradually increases. Their results imply that the WPA emerges in response to interaction between localized forcing by monsoon and the mid-latitude baroclinic eddies. Furthermore, Kosaka and Nakamura (2006) aruged that the emergence of the Bonin high can be attributed to the western Paci c convective heating, contradicting the conclusion of Enomoto et al. (2003). The teleconnection between the convective activity in the tropical western Paci c and the upper-level anticyclone anomaly over Japan is called the \Paci c-Japan (PJ) pattern" (Nitta, 1987). R. Lu and Lin (2009) employed a baroclinic model and suggested that the latent heating released from the rainfall anomalies near the Philippine Sea facilitates the eastward wave propagation towards Japan and forms the WPA. Similarly, Ren et al. (2015) showed that the diabatic heating induced by enhanced rainfall over the south China Sea initiates the eastward extension of the AMA. In addition, Kosaka et al. (2009) applied the empirical orthogonal function on monthly-mean 200 hPa meridional winds spanning over the Asian monsoon regions and indicated that the SR pattern and the PJ pattern coincide. Chen and Huang (2012) performed an SVD analysis between upper-level meridional wind across Asia and tropical rainfall on monthly scales and identi ed that the SR pattern also includes a signature of the PJ pattern. Thus, previous research has concluded that several di erent mechanisms can contribute to enhancement of the WPA, and our goals include revisiting these mechanisms in the context of transient WPA events. Moreover, the WPA has been mostly examined in the context of monthly and seasonal time scales, but the transient behavior of the WPA associated with eastward eddy shedding has not been fully analyzed.

In this study, we examine the dynamical mechanisms of eastward eddy shedding associated with the formation of WPA, in particular for transient variability. Calculations are based on the latest high resolution reanalysis products from ERA5 (section 2). In section 3, we first analyze the statistical occurrence of enhanced Bonin high events and isolated large amplitude WPA, and their relationships to eastward eddy shedding. Composite patterns of large WPA are analyzed to illustrate the time evolution of shedding events. We define an index to measure the strength of the Bonin high, select isolated large amplitude WPA events, and quantify links with the SR and the PJ patterns, respectively. The dynamics of eastward shedding are then thoroughly investigated with the help of these indices. The goal is to incorporate the synoptic eddy regime into the existing literature. Section 4 concludes the paper.

2 Reanalysis data

We use European Centre for Medium-Range Weather Forecasts (ECMWF) ERA5 meteorological products (Hersbach et al., 2020), including geopotential (z), potential vorticity, zonal and meridional (u and v) wind fields, and temperature. We employ top net thermal radiation (the negative of outgoing longwave radiation, OLR) as a proxy for deep convection. Reanalyses are used at 6-hourly intervals (0000, 0600, 1200, and 1800 UTC) with a horizontal resolution of 0.25° latitude $\times$ 0.25° longitude on 37 standard pressure levels. Our investigation focuses on the eastward eddy shedding at 100 hPa during the months of July–August over forty-one years (1979–2019).

3 Results

3.1 Overview of the WPA

Several previous studies of the Asian summer anticyclone identified a single maximum along the geopotential ridge line and found a bimodality behavior, referred to as the Tibetan Plateau (TP) mode and the Iranian Plateau (IP) mode (Q. Zhang et al., 2002; Nützel et al., 2016). Honomichl and Pan (2020) identified multiple simultaneous anticyclonic circulation centers at 100 hPa, and highlighted frequent occurrence of a third center over the western Pacific. We follow their method to identify localized anticyclones, slightly modifying the

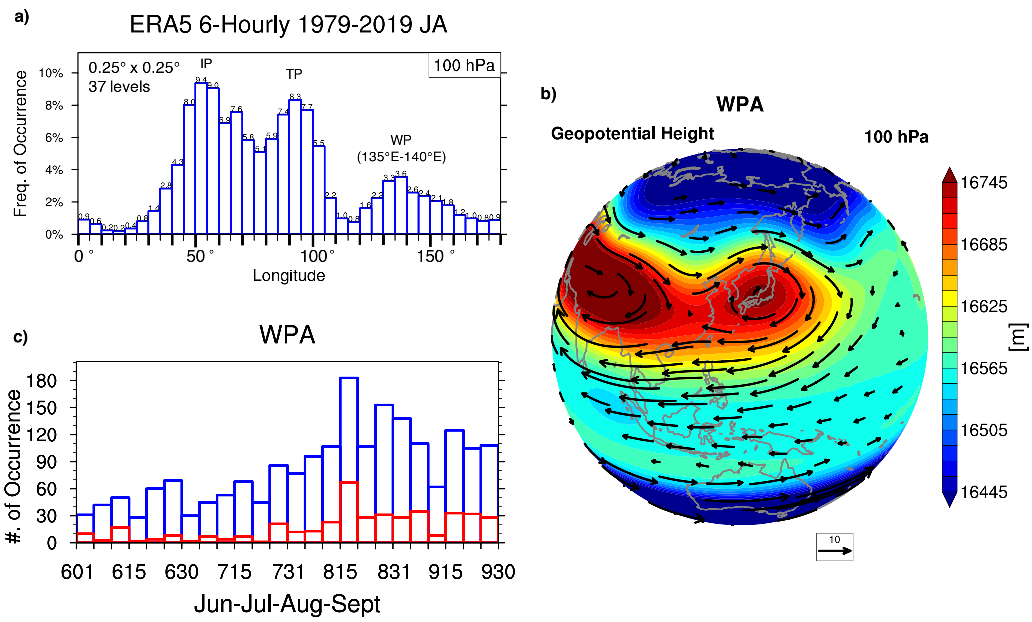

Figure 1. (a) The frequency distribution of the anticyclone centers vs. longitude at 100 hPa compiled using ERA5 6-hourly Geopotential during July-August, 1979-2019 (2542 days in total). Values above each bar indicate the frequency of occurrence in (numbers/2542 days). \IP" refers to the Iranian Plateau mode, \TP" refers to the Tibetan Plateau mode, and \WP" refers to the western Paci c mode. (b) 100 hPa geopotential height (in colors, m) and horizontal circulation (in arrows, m= s) for composites associated with WPA events. (c) The distribution of WPA occurrence dates during June to September of 1979-2019. Blue bars indicate overall histograms while red bars indicate stronger anticyclonic events when the v wind threshold is 6 m= s

details to eliminate any localized small-scale circulations in the higher resolution ERA5 data. Specifically, maxima are selected only if the meridional wind within 1500 km of the center along the ridge was greater than 3 (-3) on the west (east) side. Note that we have adopted a more strict criterion (3 vs. 0 threshold as in Honomichl & Pan, 2020) for selecting local maxima due to the finer horizontal grid resolution of ERA5 than ERA-Interim. Fig. 1a shows the histogram of frequency and longitude of transient anticyclone centers at 100 hPa for July–August. In addition to the IP mode near 50 E and TP mode near 90 E, a third preferred center is found over the western Pacific (WP) peaking around 135-140 E. The frequency distribution is almost identical to the previously calculated result (Fig. 3a, Honomichl & Pan, 2020), and similar to the results of Siu and Bowman (2020). We've repeated the analysis on meteorological fields at 150 hPa level and found that the locations for the WPA remain the same (not shown).

To gain a better understanding of the dynamical processes leading to the eastward eddy shedding, we define the WPA event as anticyclonic center that falls within the 135 -140 E longitudinal bin during July-August. This analysis selects 614 samples using 6-hourly data over 41 years and construct 100 hPa geopotential composite; these 614 samples represent 140 seperate events during 1979-2019, i.e. typically 3-4 events per year. As displayed in Fig. 1b, a localized maximum of geopotential and associated meridional winds identifies a separate anticyclone is prominent in the western Pacific region, adjacent to the AMA. Figure 1c shows the number of WPA events during June to September during 1979-2019, suggesting that the occurrence of WPA peaks in late August and drops in September. Sensitivity test shows that doubling the v wind criterion to 6 , i.e., selecting stronger localized anticyclones, doesn't change the shape of the distribution as indicated by red bars. We note that the distribution of anticyclonic centers for June-September is similar to that in Fig. 1a (not shown), and the composited signals are about the same as for July-August.

To quantify the strength of the anticyclone over Japan, a Bonin high Index (BHI) is defined as the regional averaged geopotential height within 30-55 N and 135 -140 E. Figure 2 shows time series of the BHI during July and August 1979-2019, along with identified WPA events. The curves exhibit substantial intraseasonal and yearly variabilities in frequency and intensity. Overall, the WPA events typically coincide well with peaks in BHI, although not for all events. It is because we require the WPA to be an anticyclonic cell while the BHI does not indicate a closed contour, e.g., a strong ridge can create large BHI but not WPA.

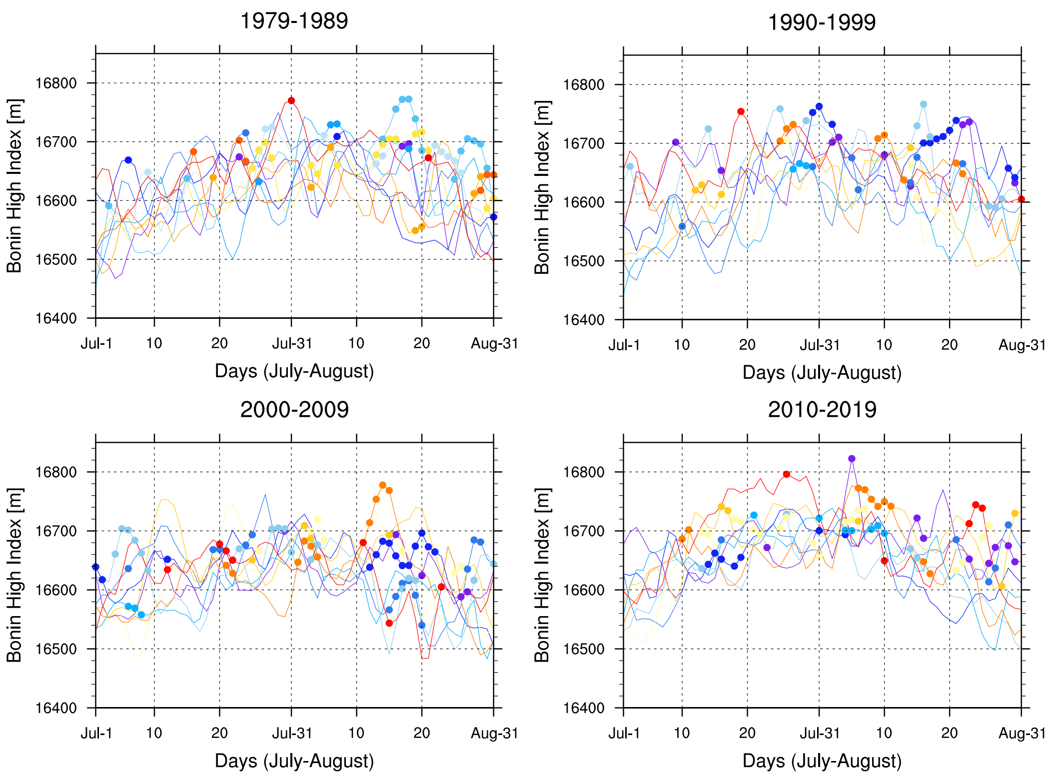

Figure 2. The color curves show the time series of the BHI in July-August over 41 years. Each color curve represent one year. Colored dots indicate the identi ed WPA events.

The 100 hPa geopotential and meridional wind anomalies composited for the WPA events are shown in Fig. 3a and b, respectively. We subtract the climatological mean value for each time step to derive a deseasonalized anomaly. Here Day 0 denotes the day the WPA event occurs. The composited wave packet structure shows disturbances embedded along the climatological westerly ow with an approximate zonal scale of wavenumber 6. Positive geopotential coupled with intensi ed anticyclone occurs near the jet exit above Japan. The composite features are not sensitive to the choice of the longitude range in de ning the WPA events (not shown). Time development of geopotential height averaged over 40-45 N along the upper-level jet at 100 hPa is depicted by the Hovmoller diagram in Fig. 3c, highlighting coherent upstream wave structure beginning 4 days prior to the WPA events. The wave packet has near zero phase velocity, but a clear eastward group velocity near 24 . The wave packet propagates downstream through the waveguide of the jet core, and ampli es near the jet exit on Day 0. The quasi-stationary zonal wavenumber 6 structure identi ed in Fig. 3 is consistent with the SR behavior analyzed in Kosaka et al. (2009), interpreted as a stationary Rossby wave on the background westerly jet. During Day +1 to +4, wave packets develop successively downstream and reach the Paci c coast of the United States.

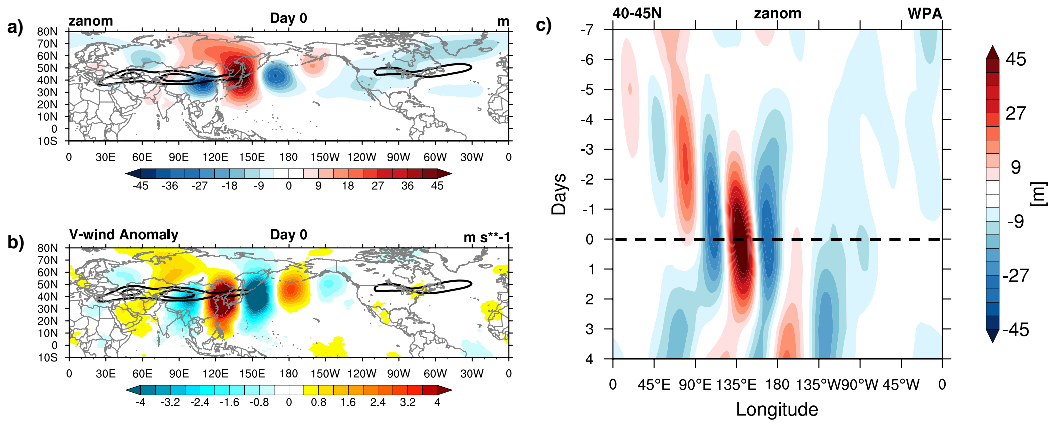

Figure 3. Composites of 100 hPa geopotential and meridional wind anomalies (zanom and vanom) for the WPA events on Day 0 in (a) and (b), respectively. Regions where anomalies are not signi cant at the 95% level using t-test are shaded white. Black contours highlight the 200 hPa climatological westerly jet of 24 and 30 m=s (c) Hovmoller diagram of zanom at 100 hPa averaged over 40 -45 N from Day -7 to +4.

Fig. 4a displays the time evolution of PV interpolated to 360 K isentrope for the composited WPA events. The anticyclone is associated with a region of relatively low PV,

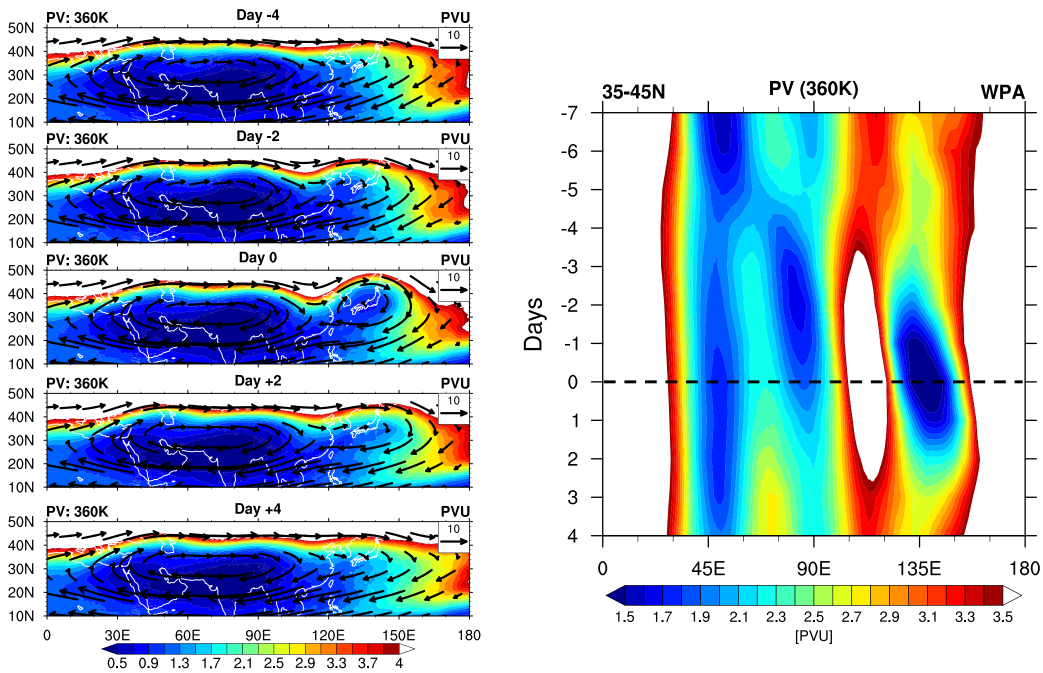

Figure 4. (a) Composite patterns of PV (in colors, PVU) at 360 K overlaid with the winds at 100 hPa (in vectors, m/s) on Day -4, Day -2, Day 0, Day +2, and Day +4 of the WPA events, respectively. (b) Hovmoller diagram of PV at 360 K averaged over 35 -45 N from Day -7 to Day +4.

e.g. Garny and Randel (2016) and Ploeger et al. (2017). Low PV patches develop on the eastern side of the anticyclone during the WPA events, in a manner consistent with wave trains seen in Fig. 3. Fig. 4b shows a Hovmöller diagram of PV at 360 K averaged over 35-45 N from Day -7 to +4, highlighting development of low PV air over the composite WPA life cycle. During Day -4 to +2, the low PV air associated with the eastward shedding is confined between 120-150 E and remains quasi-stationary, consistent with the geopotential signature in Fig. 3. The PV evolution is consistent with the developing WPA transporting air masses with elevated mixing ratios of CO and H_2O rapidly into the extratropical lower stratosphere (Ploeger et al., 2015; Pan et al., 2016). We note that while the WPA is quasi-stationary, air parcel trajectories can move through the circulation and transport constituents towards the east, e.g. Honomichl and Pan (2020), their Fig. 7.

The composited WPA meteorological features include combined effects of the SR and PJ teleconnections – wave trains in the upper troposphere together with enhanced convection over the tropical western Pacific (Fig. S1). However, the SR and PJ patterns do not always coincide in individual cases, which motivates us to evaluate the WPA events in terms of relations to the SR and PJ indices and examine their dynamics separately.

3.2 WPA Relationships to the Silk Road Pattern

[illegible]

The most striking feature in Fig. 3 is the quasi-stationary wave along the upper-level jet, resembling the SR pattern (R.-Y. Lu et al., 2002; Enomoto et al., 2003). To quantify the occurrence of the Silk Road wave trains, we construct a time varying Silk Road Index (SRI). As indicated by the composite map of geopotential height averaged over Day -4 to -1 preceding the WPA events in Fig. 5, we see that the SR pattern consists of four zonally oriented anomaly centers confined to 35-55 N, located over A the Caspian Sea (40-55 E), B central Asia (70 -85 E), C Mongolia (95 -115 E), and D east China (120 -140 E). Two negative geopotential centers are marked as A and C while two positive centers are marked as B and D. We define z_i as the maximum anomaly value in each box and SRI is the sum of absolute values of the four boxes as in Eq. 1:

$$SRI = \sum_{i=A;C} z_i + \sum_{i=B;D} z_i \qquad (1)$$

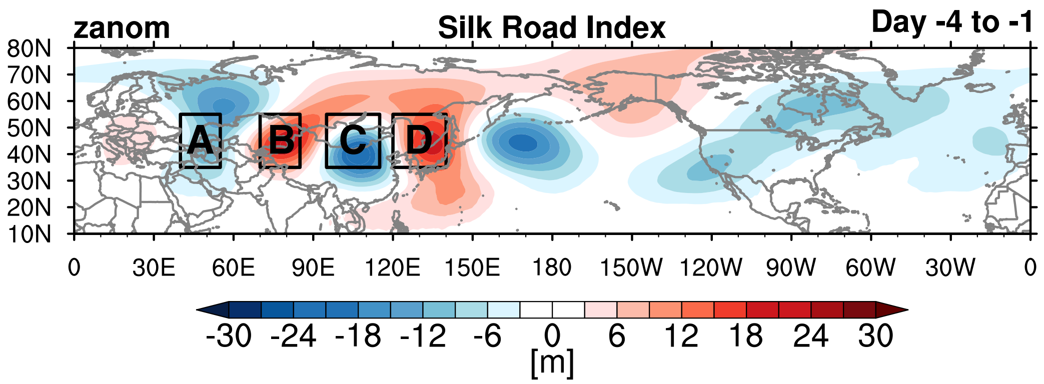

Figure 5. Schematic illustrating four centers where the SRI is constructed. The zanom composites (in colors) are averaged during Day -4 to -1 prior to the WPA events.

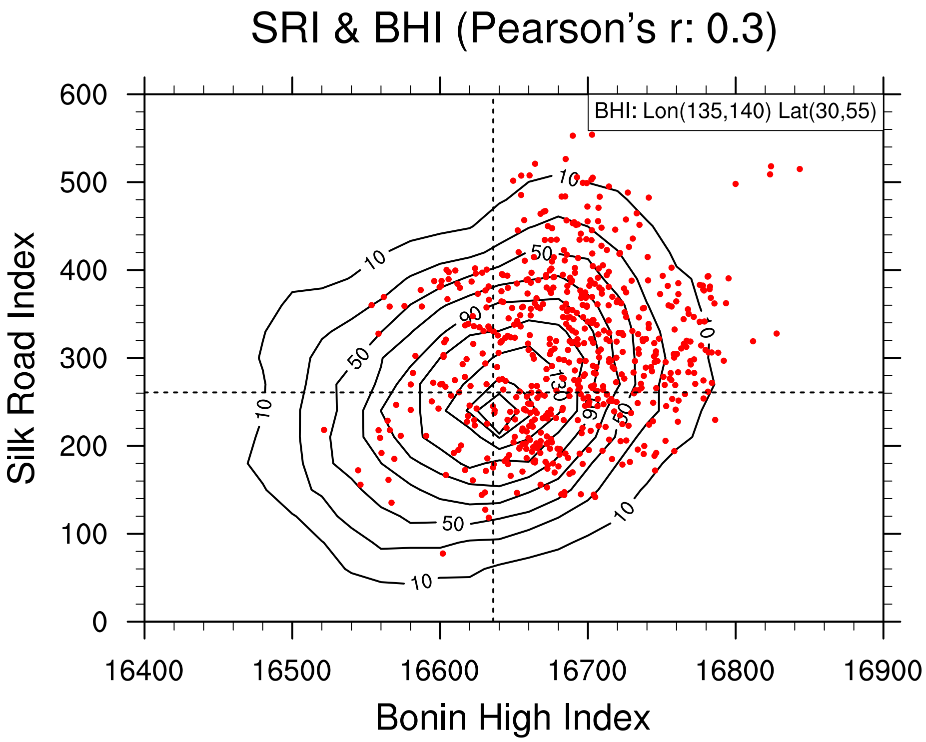

Figure 6. Two dimensional distribution of the SRI against the BHI compiled using all July-August data during 1979-2019. Red dots indicate the WPA events. Dashed reference lines indicate the median values. Correlation coe cient is given in the gure title.

Figure 6 shows a 2D distribution of SRI vs. BHI for all daily samples over July-August 1979-2019. Contours represent the density of scatter points. There is a weak but statistically signi cant correlation in the distribution (r 0:3), as expected from the results in Fig. 3. The red dots in Fig. 6 represent the WPA events, primarily falling in the upper right-hand quadrant, i.e. large amplitude BHI and SRI. These statistics are consistent with an ampli ed Silk Road pattern typically preceding the strong anticyclone above Japan by 1 to 4 days.

3.2.2 Dynamics in Relation to the Silk-Road Pattern

We apply composite analysis to obtain the essential circulation patterns of the WPA with reference to the intensity of the SR pattern. To sharpen the composited features, variables whose SRI fall above the 75th percentile are selected. Wave activity ux (WAF) vectors are computed to identify the origin and propagation of Rossby waves associated with the WPA events coinciding with the pronounced SR pattern. The calculation is based on the methods of Takaya and Nakamura (2001), which generalizes Plumb uxes (Plumb, 1979) to allow for transient eddies propagating in a zonally varying mean state. The WAF is designed in the quasi-geostrophic (QG) framework, whose direction is parallel to the wave group velocity and the divergence (convergence) implies source (sink) of Rossby waves (H.-H. Hsu & Lin, 2007; Gu et al., 2018).

Figure 7. Cross sections of QG streamfunction anomalies (in colors, unit: 10^{6} m^2=s) and WAF (in vectors, unit: m^2=s^2) (a) averaged over 120 -140 E and (b) at 40 N composited for the WPA events which coincide with pronounced Silk Road pattern.

statistical significance at the 95% confidence level), although there is stronger relationship for extreme PJ patterns. For instance, red dots represent the WPA events whose PJI falls above the 75th percentile and suggest a positive correlation with the intensity of the WPA. Figure 11b shows only the significant correlation coefficients between the PJI and the BHI as the PJI increases from -30, -20, ..., 20, 30W=m^2. The correlation is in fact maximized when the PJI falls above the upper 30th percentile (0.47*) while becomes insignificant as the PJI reaches 20W=m^2. The upper 30th percentile agrees well with statistics of back trajectories initialized within the WPA in Honomichl and Pan (2020), where one third of air parcels trace back to the Philippine Sea.

Figure 11. (a) Scatterplot between the BHI (m) against the PJI (W=m^2) composited for a total of 614 Bonin high events. Red dots highlight the Bonin high events whose PJI falls above the 75th percentile. Correlation coefficients are given in the figure title. Gray reference lines indicate the 10th (p10), the 25th (p25), the median (p50), the 67th (p67), the 75th (p75), and the 90th (p90) percentiles of the PJI, respectively. (b) Curve indicates the significant correlation between subsets of the BHI and PJI, which are regrouped as the PJI increases.

3.3.2 Dynamics in Relation to the Pacific-Japan Pattern

We apply composite analysis to identify the circulation patterns with reference to the intensity of the PJ pattern. Similar to Section 3.2.2, variables composited for the WPA events on Day 0 are averaged when the corresponding PJI falls above the 75th percentile, i.e. enhanced convection as in Fig. 10a (represented by gray contours in Fig. 12b). Fig. 12a

the Far East. Acta Meteorologica Sinica, 34(4), 385{396.

Vernier, J.-P., Fairlie, T., Natarajan, M., Wienhold, F., Bian, J., Martinsson, B., . . . Bedka, K. (2015). Increase in upper tropospheric and lower stratospheric aerosol levels and its potential connection with asian pollution. Journal of Geophysical Research: Atmospheres, 120(4), 1608{1619.

Vogel, B., Günther, G., Müller, R., Grooß, J., Hoor, P., Krämer, M., . . . Riese, M. (2014). Fast transport from Southeast Asia boundary layer sources to northern Europe: rapid uplift in typhoons and eastward eddy shedding of the Asian monsoon anticyclone. Atmos. Chem. Phys, 14(23), 12{745.

Wang, B. (1994). Climatic regimes of tropical convection and rainfall. Journal of Climate, 1109{1118.

Wang, B., & Fan, Z. (1999). Choice of South Asian summer monsoon indices. Bulletin of the American Meteorological Society, 80(4), 629{638.

Wang, X., Wu, Y., Tung, W.-w., Richter, J. H., Glanville, A. A., Tilmes, S., . . . Kinnison, D. E. (2018). The Simulation of Stratospheric Water Vapor Over the Asian Summer Monsoon in CESM1 (WACCM) Models. Journal of Geophysical Research: Atmospheres, 123(20), 11{377.

Wu, L., Chou, C., Chen, C.-T., Huang, R., Knutson, T. R., Sirutis, J. J., . . . Feng, Y.-C. (2014). Simulations of the present and late-twenty-first-century western North Pacific tropical cyclone activity using a regional model. Journal of Climate, 27(9), 3405{3424.

Wu, Y., Orbe, C., Tilmes, S., Abalos, M., & Wang, X. (2020). Fast Transport Pathways Into the Northern Hemisphere Upper Troposphere and Lower Stratosphere During Northern Summer. Journal of Geophysical Research: Atmospheres, 125(3), e2019JD031552.

Yamada, K., & Kawamura, R. (2007). Dynamical link between typhoon activity and the PJ teleconnection pattern from early summer to autumn as revealed by the JRA-25 reanalysis. SOLA, 3, 65{68.

Yasui, S., & Watanabe, M. (2010). Forcing processes of the summertime circumglobal teleconnection pattern in a dry AGCM. Journal of Climate, 23(8), 2093{2114.

Zhang, P., Liu, Y., & He, B. (2016). Impact of East Asian summer monsoon heating on the interannual variation of the South Asian high. Journal of Climate, 29(1), 159{173.

Zhang, Q., Wu, G., & Qian, Y. (2002). The bimodality of the 100 hPa South Asia High and its relationship to the climate anomaly over East Asia in summer. Journal of the

596 Meteorological Society of Japan. Ser. II, 80(4), 733{744.